Article DOI: https://doi.org/10.3201/eid2512.190504

# Genetic Characterization of Avian Influenza A(H5N6) Virus Clade 2.3.4.4, Russia, 2018

## Appendix

### Measurement of Equilibrium Dissociation Constants

To determine receptor preference, we measured binding kinetics of virions to receptor analogs by surface plasma resonance on a ProteOn XPR36 (Bio-Rad, https://www.bio-rad.com) with a NeutrAvidin chip (Bio-Rad) and 3′-Sialyl-N-acetyllactosamine and 6′-Sialyl-N-acetyllactosamine biotinylated receptor analogs (Dextra, https://www.dextrauk.com). We immobilized α2–3 and α2–6 glycans on the NLC chip in sodium phosphate buffer (pH 7.4) at a concentration of 100 μg/mL. We injected 5 dilutions of purified virus sample in the same buffer at a flow rate of 70 μL/min with 350 seconds contact time for association. Dissociation lasted 600 seconds at the same flow rate. We added oseltamivir (20 nmol/L) to inhibit neuraminidase. We analyzed data with the ProteOn Manager (Bio-Rad) software using Langmuir kinetics calculations model (Appendix Figure 9). We calculated equilibrium dissociation constants ($K_D$) as ratio of dissociation and association constants: $K_D = k_d/k_a$. We used 3 independent surface plasma resonance runs to verify the equilibrium dissociation constants.

$K_D$ for 3′SLN and 6′SLN of A/common gull/Saratov/1676/2018

$K_D$ for 3′SLN = 12.2 ± 0.7 nmol/L

$K_D$ for 6′SLN = 43.3 ± 2.8 nmol/L

$K_D$ for 3′SLN and 6′SLN of A/rook/Chany/32/2015

$K_D$ for 3′SLN = 0.2 ± 0.02 μmol/L

$K_D$ for 6′SLN = 6.3 ± 0.1 μmol/L

The data confirms preferential binding of both strains to α2,3-SA.

**Appendix Table 1**. Comparison of gene segments of avian influenza A(H5N6) virus clade 2.3.4.4 isolated in Russia, 2018 with human influenza A H5N6 viruses*

| Gene segment | GISAID no. | Guangxi/32797/ 2018 | Guangxi/31906/ 2018 | Guangdong/ 18SF020/2018 | Guangxi/13486/2017 | Jiangsu/32888/2018 |
|---|---|---|---|---|---|---|
| HA | EPI1355418 | 1,763/1,773 (99) | 1,753/1,772 (98) | 1,753/1,774 (98) | 1,744/1,774 (98) | 1,723/1,775 (97) |
| NA | EPI1355420 | 1,430/1,432 (99) | 1,416/1,432 (98) | 1,411/1,432 (98) | 1,418/1,432 (99) | 1,378/1,435 (96) |
| PB2 | EPI1355415 | 2,330/2,335 (99) | 2,324/2,341 (99) | 2,303/2,326 (99) | 2,303/2,326 (99) | 2,283/2,326 (98) |
| PB1 | EPI1355416 | 2,290/2,301 (99) | 2,310/2,341 (98) | 2,237/2,274 (98) | 2,256/2,274 (99) | 2,300/2,331 (98) |
| PA | EPI1355417 | 2,225/2,233 (99) | 2,209/2,233 (98) | 2,123/2,151 (98) | 2,132/2,151 (99) | 2,017/2,214 (91) |
| NP | EPI1355419 | 1,540/1,543 (99) | 1,548/1,565 (98) | 1,550/1,565 (99) | 1,551/1,565 (99) | 1,550/1,565 (99) |
| M | EPI1355421 | 1,022/1,027 (99) | 1,018/1,027 (99) | 1,024/1,028 (99) | 1,003/1,012 (99) | 1,018/1,027 (99) |
| NSP | EPI1355422 | 868/870 (99) | 865/875 (98) | 870/875 (99) | 872/875 (99) | 871/876 (99) |

*Avian influenza A(H5N6) isolated in this study, A/common gull/Saratov/1676/2018 in Global Initiative on Sharing All Influenza Data database. Values for nucleic sequence homology of each gene segment expressed as gene segments of A/common gull/Saratov/1676/2018 versus gene segments of human A(H5N6). Values in parentheses represent % identity. GSAID, Global Initiative on Sharing All Influenza Data HA, hemagglutinin; M, matrix; NA, neuraminidase; NP, nucleoprotein; NSP, nonstructural protein; PA, polymerase; PB1, polymerase basic 1; PB2, polymerase basic 2.

**Appendix Table 2.** Amino acid changes in proteins of avian influenza A(H5N6) compared with the closest homologue and H5N6 candidate vaccine viruses*

| | Human H5N6 virus strains | | | | Avian H5N6 virus strains | | | |
|---|---|---|---|---|---|---|---|---|
| Gene | A/Hubei/ 29578/ 2016† | A/Fujian-Sanyuan/ 21099/ 2017† | A/Sichuan/ 26221/ 2014† | A/Guangxi/ 32797/ 2018† | A/chicken/ Vietnam/ NCVD-15A59/2015† | A/duck/ Hyogo/ 1/2016† | A/common gull/ Saratov/ 1676/2018 | Phenotypic characteristics |
| HA (H5 no.) | | | | | | | | |
| D54N | D | D | D | N | D | D | N | Creates a potential N-glycosylation site |
| D94N | N | S | N | N | N | N | N | Increased virus binding to α2–6 |
| L115Q | L | L | L | Q | L | L | Q | Antigenic drift |
| S121Y | S | S | S | S | S | S | Y | Together with I151T antigenic drift |
| S123P | P | P | T | S | P | P | S | Increased virus binding to α2–6 |
| 126 Del | Del | E | E | Del | E | E | Del | Creates a potential N-glycosylation site |
| L129S | S | L | L | S | L | Del | S | Position associated with antigenic drift |
| S133A | A | A | A | A | A | A | A | Increased virus binding to α2–6 |
| L/Q138T | L | Q | Q | T | Q | Q | T | Position associated with antigenic drift |
| K/M/T140V | K | T | T | V | M | V | V | Position associated with antigenic drift |
| P141A | P | P | P | A | P | P | A | Antigenic drift |
| I151T | T | I | I | T | T | T | T | With S121Y, antigenic drift; with 129Del, host specificity shift |
| T156A | A | A | A | A | A | A | A | Increased virus binding to α2–6 |
| N183S | N | N | N | S | N | N | S | Position associated with antigenic drift, host specificity shift |
| T188A | T | T | T | A | T | T | A | Host specificity shift |
| N189D | N | N | N | D | N | N | D | Antigenic drift |
| 220–224 | NGQSG | NGQRG | NGQRG | NGQHG | NGQRG | NGQQG | NGQRG | 222–224 QS(R)G avian-like α2–3 receptor-binding preference |
| A263T | T | T | T | T | T | T | T | Increased virulence in mammals |
| Cleavage peptides | RERRRKR | REKRRKR | REKRRKR | RERRRKR | RERRRKR | RERRRKR | RERRRKR | Highly pathogenic avian influenza |
| NA (N6 no.) | | | | | | | | |
| 59–69 Del | yes | yes | no | yes | yes | yes | yes | Enhanced virulence in mice |
| N86K | N | K | N | K | N | K | K | Removes a potential N-glycosylation site |
| T223I | I | I | I | I | I | I | I | Increased virulence in mammals |
| PB2 | | | | | | | | |
| T63I | I | I | I | I | I | I | I | Increased virulence in mammals |
| L89V | V | V | V | V | V | V | V | Leu89Val, Gly309Asp, Thr339Lys, Arg477Gly, Ile495Val, Lys627Glu, Ala676Thr; enhanced polymerase activity and increased virulence in mice |
| G309D | D | D | D | D | D | D | D | Leu89Val, Gly309Asp, Thr339Lys, Arg477Gly, Ile495Val, Lys627Glu, Ala676Thr; enhanced polymerase activity and increased virulence in mice |
| T339K | K | K | M | K | T | K | K | Leu89Val, Gly309Asp, Thr339Lys, Arg477Gly, |

| Gene | Human H5N6 virus strains | | | | Avian H5N6 virus strains | | | Phenotypic characteristics |
|---|---|---|---|---|---|---|---|---|
| | A/Hubei/ 29578/ 2016† | A/Fujian-Sanyuan/ 21099/ 2017† | A/Sichuan/ 26221/ 2014† | A/Guangxi/ 32797/ 2018† | A/chicken/ Vietnam/ NCVD-15A59/2015† | A/duck/ Hyogo/ 1/2016† | A/common gull/ Saratov/ 1676/2018 | |
| | | | | | | | | Ile495Val, Lys627Glu, Ala676Thr; enhanced polymerase activity and increased virulence in mice |
| Q368R | R | R | Q | R | Q | R | R | Increased virulence in mammals |
| H447Q | Q | Q | Q | Q | Q | Q | Q | Increased virulence in mammals |
| R477G | G | G | G | G | G | G | G | Leu89Val, Gly309Asp, Thr339Lys, Arg477Gly, Ile495Val, Lys627Glu, Ala676Thr; enhanced polymerase activity and increased virulence in mice |
| I495V | V | V | V | V | V | V | V | Leu89Val, Gly309Asp, Thr339Lys, Arg477Gly, Ile495Val, Lys627Glu, Ala676Thr; enhanced polymerase activity and increased virulence in mice |
| A/T588V | A | A | T | V | T | V | V | Host specificity shift |
| K627E | E | E | E | K | E | E | E | Enhanced polymerase activity and increased virulence in mice, adaptation to mammals |
| A661S | A | A | A | S | A | S | S | Host specificity shift |
| A676T | M | T | T | T | T | T | T | Leu89Val, Gly309Asp, Thr339Lys, Arg477Gly, Ile495Val, Lys627Glu, Ala676Thr; enhanced polymerase activity and increased virulence in mice |
| PB1 | | | | | | | | |
| A3V | V | V | V | V | V | V | V | Increased virulence in mammals |
| L13P | P | P | P | P | P | P | P | Increased virulence in mammals |
| R207K | K | K | K | K | K | K | K | Increased virulence in mammals |
| K328N | N | N | N | N | N | N | N | Increased virulence in mammals |
| I368V | V | I | I | I | I | I | I | Increased transmission in ferrets |
| S375N | N | N | N | N | N | N | N | Increased virulence in mammals |
| H436Y | Y | Y | Y | Y | Y | Y | Y | Increased virulence in mammals |
| L473V | V | V | V | V | V | V | V | Increased virulence in mammals |
| M677T | T | T | T | T | T | T | T | Increased virulence in mammals |
| PA | | | | | | | | |
| V100A | I | V | V | V | V | V | V | Species associated signature position |
| G225S | S | S | G | S | S | S | S | Host specificity shift |
| H266R | R | R | R | R | R | R | R | Increased virulence in mammals |
| K356R | R | K | K | K | K | K | K | Species associated signature position |
| S409N | N | S | S | S | S | S | S | Species associated signature position |
| S/A515T | T | T | T | T | T | T | T | Increased virulence in mammals |
| NP | | | | | | | | |
| I33V | V | V | I | V | V | V | V | Host specificity shift |
| M1 | | | | | | | | |
| V15I | I | V | I | I | I | I | I | Increased virulence in mammals |
| N30D | D | D | D | D | D | D | D | Increased virulence in mice |
| T215A | A | A | A | A | A | A | A | Increased virulence in mice |
| M2 | | | | | | | | |
| S31N | N | S | S | S | S | S | S | Resistance to adamantine |
| S89G | G | G | S | G | G | G | G | Host specificity shift |
| NSP1 | | | | | | | | |
| P42S | S | S | S | S | S | S | S | Increased virulence in mice |
| 80–84 del | No | No | Yes | Yes | Yes | Yes | Yes | Increased virulence in mice |
| D92E‡ | D | D | E | E | E | E | E | Increased virulence in mammals |

| Gene | Human H5N6 virus strains | | | | Avian H5N6 virus strains | | | Phenotypic characteristics |
|---|---|---|---|---|---|---|---|---|
| | A/Hubei/ 29578/ 2016† | A/Fujian-Sanyuan/ 21099/ 2017† | A/Sichuan/ 26221/ 2014† | A/Guangxi/ 32797/ 2018† | A/chicken/ Vietnam/ NCVD-15A59/2015† | A/duck/ Hyogo/ 1/2016† | A/common gull/ Saratov/ 1676/2018 | |
| L98F§ | L | F | F | F | F | F | F | Increased virulence in mice |
| I101M§ | I | M | M | M | M | M | M | Increased virulence in mice |
| V149A¶ | A | A | A | A | A | A | A | Increased virulence in mammals |
| N200S§ | S | S | S | S | S | S | S | Asn200Ser, when coupled with NS2 Thr47Ala; increased virulence in mammals |
| Terminal motif ESEV | Truncated | GSEV | ESEV | ESEV | ESEV | ESEV | ESEV | Increased virulence in mice |
| NSP2 | | | | | | | | |
| T47A | A | A | A | A | A | A | A | Thr47Ala (when coupled with NS1 Asn200Ser) Increased virulence in mammals |

*Avian influenza A(H5N6) from this study, A/common gull/Saratov/1676/2018 in Global Initiative on Sharing All Influenza Data database. HA, hemagglutinin; M1, matrix 1; M2, matrix 2; NA, neuraminidase; NP, nucleoprotein; NSP1, nonstructural protein 1; NSP2, nonstructural protein 2;PA, polymerase; PB1, polymerase basic 1; PB2, polymerase basic 2.
†Candidate vaccine virus.
‡87 if the deletion is not counted.
§Deletion not counted.
¶144 if deletion not counted.

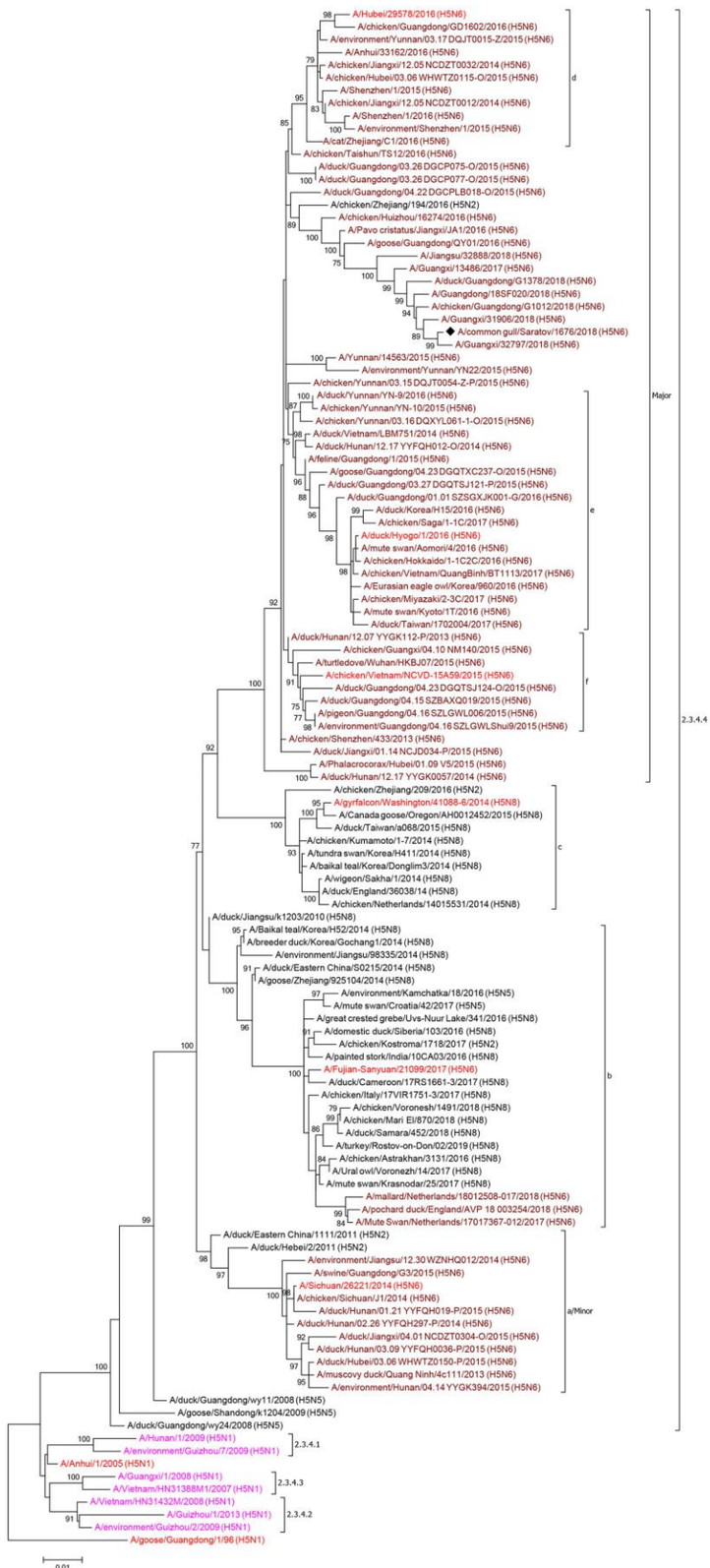


**Appendix Figure 1.** Phylogenetic analysis of the hemagglutinin (HA) gene segment of A/common gull/Saratov/1676/2018 (H5N6) isolated from a common gull (*Larus canus*) in the Saratov Region of Russia, 2018. Phylogenetic analysis was performed by using MEGA version 6.0 (http://www.megasoftware.net) and the maximum likelihood method with 500 bootstrap replications. Genetic clusters of avian influenza viruses are annotated by brackets. Numbers near the branches indicate bootstrap value >70%. Influenza virus sequences were deposited in Global Initiative on Sharing All Influenza Data (GISAID; https://platform.gisaid.org/epi3) under identification no. EPI1355418. Sequence data from the Influenza Research Database (IRD; https://www.fludb.org) and GenBank (https://www.ncbi.nlm.nih.gov/genbank) were used for comparison. Black diamond indicates isolate from this study. Red text indicates candidate vaccine viruses. Blue text indicates H9N2/H7N9 sequences; green text indicates H6 subtypes; pink text indicates H5N1 subtypes; brown text indicates H5N6 subtypes. Scale bar indicates nucleotide substitutions per site.

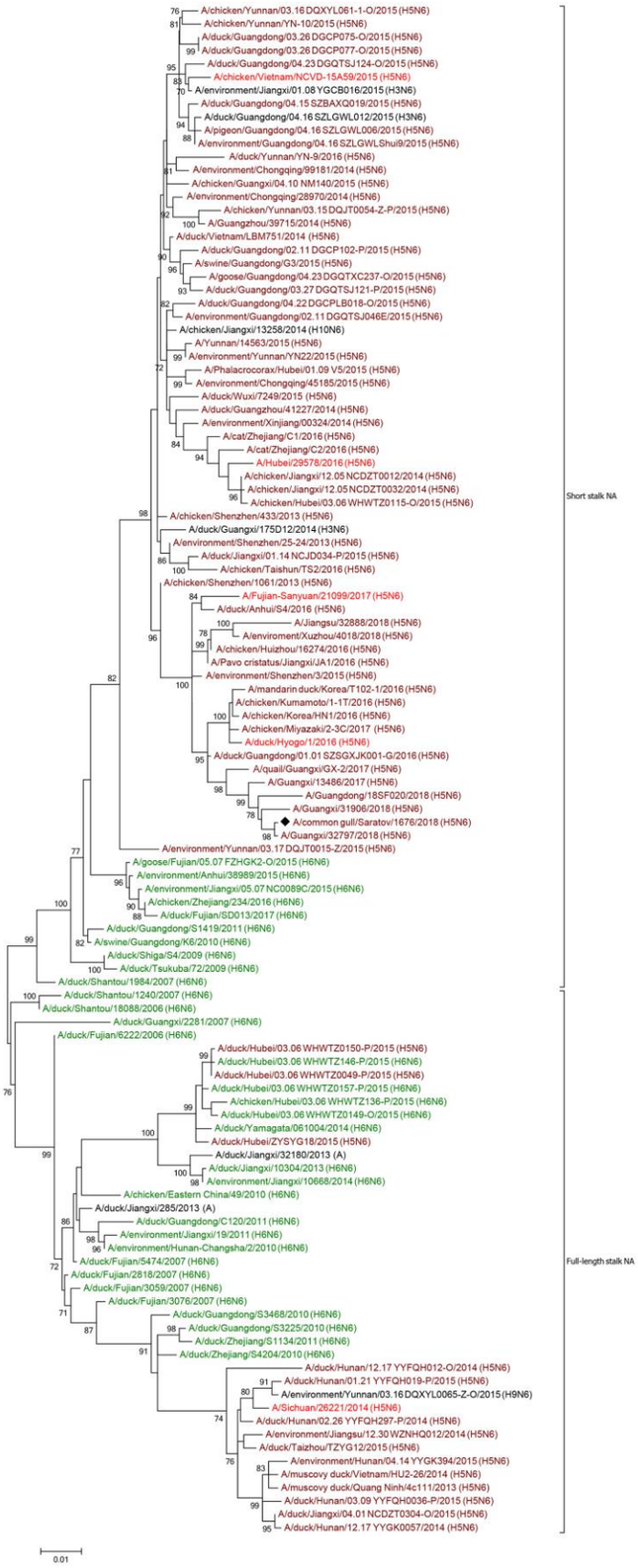


**Appendix Figure 2.** Phylogenetic analysis of the neuraminidase (NA) gene segment of A/common gull/Saratov/1676/2018 (H5N6) isolated from a common gull (*Larus canus*) in the Saratov Region of Russia, 2018. Phylogenetic analysis was performed by using MEGA version 6.0 (http://www.megasoftware.net) and the maximum likelihood method with 500 bootstrap replications. Genetic clusters of avian influenza viruses are annotated by brackets. Numbers near the branches indicate bootstrap value >70%. Influenza virus sequences were deposited in Global Initiative on Sharing All Influenza Data (GISAID; https://platform.gisaid.org/epi3) under identification no. EPI1355418. Sequence data from the Influenza Research Database (IRD; https://www.fludb.org) and GenBank (https://www.ncbi.nlm.nih.gov/genbank) were used for comparison. Black diamond indicates isolate from this study. Red text indicates candidate vaccine viruses. Blue text indicates H9N2/H7N9 sequences; green text indicates H6 subtypes; pink text indicates H5N1 subtypes; brown text indicates H5N6 subtypes. Scale bar indicates nucleotide substitutions per site.

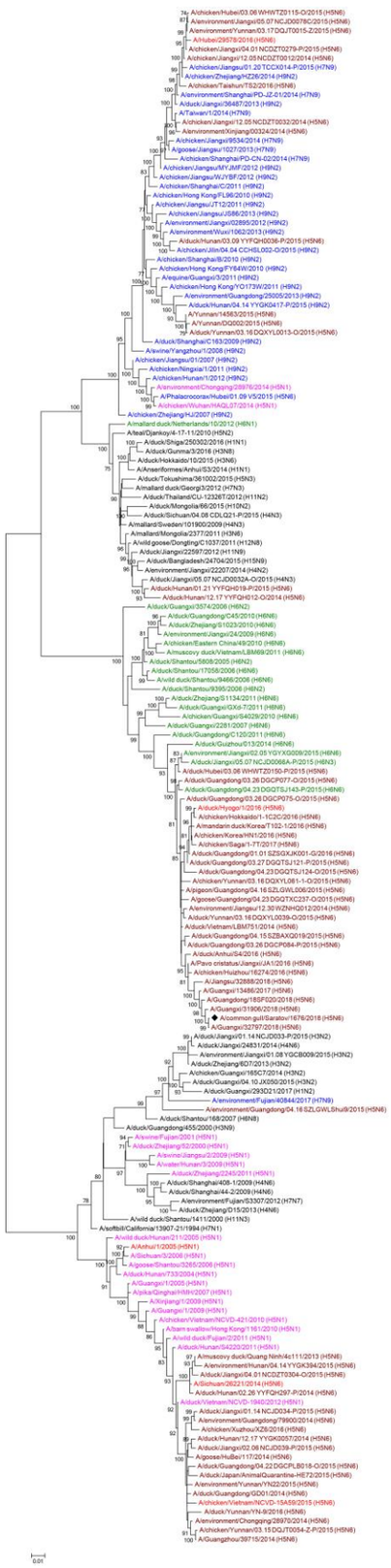

**Appendix Figure 3.** Phylogenetic analysis of the polymerase basic protein 2 (PB2) gene segment of A/common gull/Saratov/1676/2018 (H5N6) isolated from a common gull (*Larus canus*) in the Saratov Region of Russia, 2018. Phylogenetic analysis was performed by using MEGA version 6.0 (http://www.megasoftware.net) and the maximum likelihood method with 500 bootstrap replications. Numbers near the branches indicate bootstrap value >70%. Influenza virus sequences were deposited in Global Initiative on Sharing All Influenza Data (GISAID; https://platform.gisaid.org/epi3 under identification no. EPI1355418. Sequence data from the Influenza Research Database (IRD; https://www.fludb.org) and GenBank (https://www.ncbi.nlm.nih.gov/genbank) were used for comparison. Black diamond indicates isolate from this study. Red text indicates candidate vaccine viruses. Blue text indicates H9N2/H7N9 sequences; green text indicates H6 subtypes; pink text indicates H5N1 subtypes; brown text indicates H5N6 subtypes. Scale bar indicates nucleotide substitutions per site.

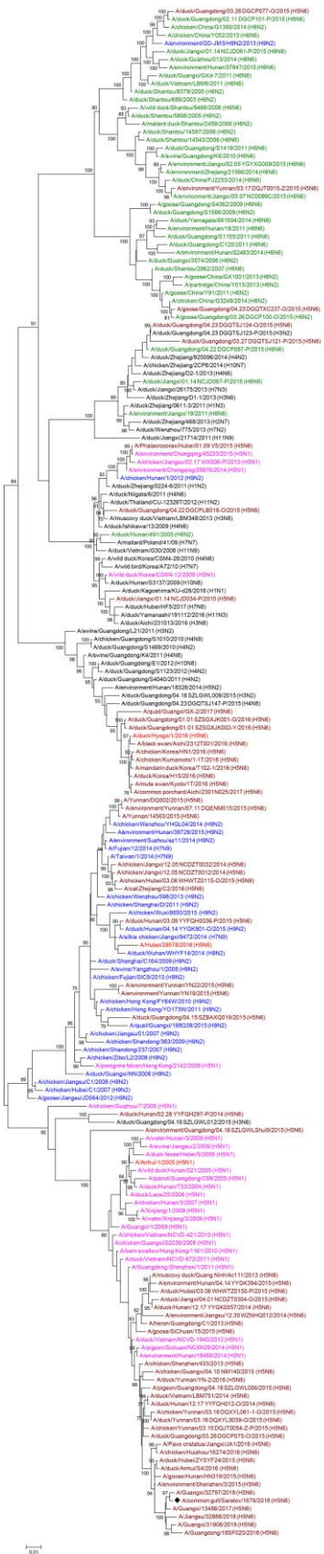

**Appendix Figure 4.** Phylogenetic analysis of the polymerase basic protein 1 (PB1) gene segment of A/common gull/Saratov/1676/2018 (H5N6) isolated from a common gull (*Larus canus*) in the Saratov Region of Russia, 2018. Phylogenetic analysis was performed by using MEGA version 6.0 (http://www.megasoftware.net) and the maximum likelihood method with 500 bootstrap replications. Numbers near the branches indicate bootstrap value >70%. Influenza virus sequences were deposited in Global Initiative on Sharing All Influenza Data (GISAID; https://platform.gisaid.org/epi3) under identification no. EPI1355418. Sequence data from the Influenza Research Database (IRD; https://www.fludb.org) and GenBank (https://www.ncbi.nlm.nih.gov/genbank) were used for comparison. Black diamond indicates isolate from this study. Red text indicates candidate vaccine viruses. Blue text indicates H9N2/H7N9 sequences; green text indicates H6 subtypes; pink text indicates H5N1 subtypes; brown text indicates H5N6 subtypes. Scale bar indicates nucleotide substitutions per site.

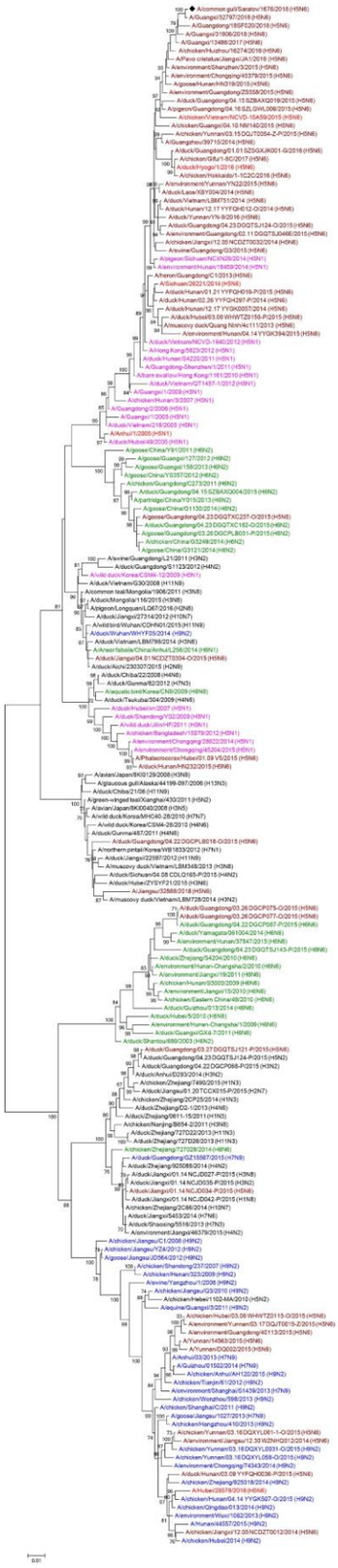

**Appendix Figure 5.** Phylogenetic analysis of the polymerase acidic (PA) gene segment of A/common gull/Saratov/1676/2018 (H5N6) isolated from a common gull (*Larus canus*) in the Saratov Region of Russia, 2018. Phylogenetic analysis was performed by using MEGA version 6.0 (http://www.megasoftware.net) and the maximum likelihood method with 500 bootstrap replications. Numbers near the branches indicate bootstrap value >70%. Influenza virus sequences were deposited in Global Initiative on Sharing All Influenza Data (GISAID; https://platform.gisaid.org/epi3) under identification no. EPI1355418. Sequence data from the Influenza Research Database (IRD; https://www.fludb.org) and GenBank (https://www.ncbi.nlm.nih.gov/genbank) were used for comparison. Black diamond indicates isolate from this study. Red text indicates candidate vaccine viruses. Blue text indicates H9N2/H7N9 sequences; green text indicates H6 subtypes; pink text indicates H5N1 subtypes; brown text indicates H5N6 subtypes. Scale bar indicates nucleotide substitutions per site.

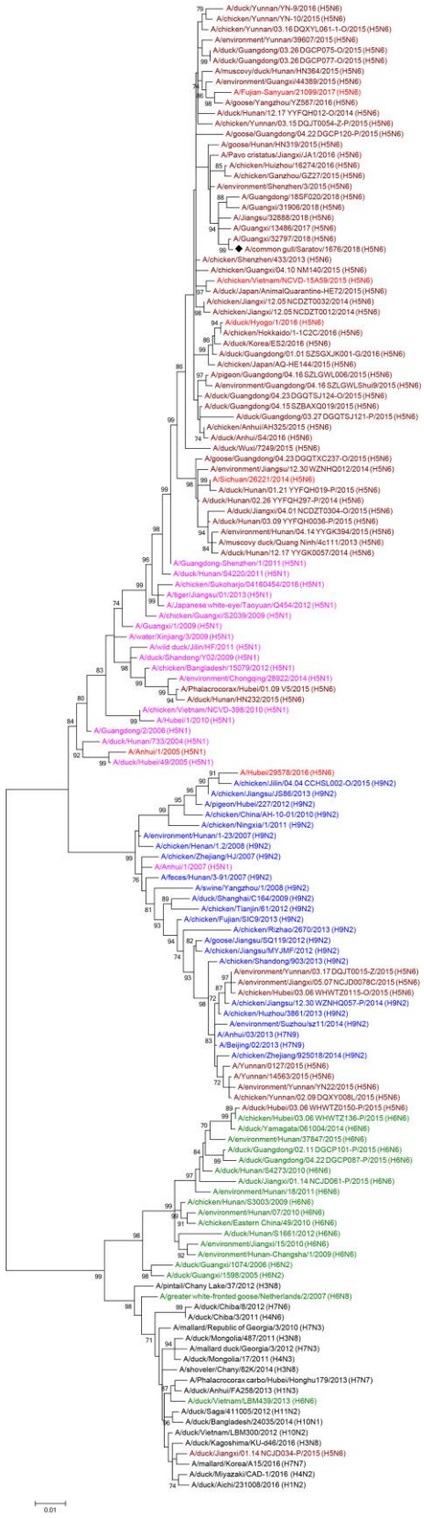


**Appendix Figure 6.** Phylogenetic analysis of the nucleoprotein (NP) gene segment of A/common gull/Saratov/1676/2018 (H5N6) isolated from a common gull (*Larus canus*) in the Saratov Region of Russia, 2018. Phylogenetic analysis was performed by using MEGA version 6.0 (http://www.megasoftware.net) and the maximum likelihood method with 500 bootstrap replications. Numbers near the branches indicate bootstrap value >70%. Influenza virus sequences were deposited in Global Initiative on Sharing All Influenza Data (GISAID; https://platform.gisaid.org/epi3) under identification no. EPI1355418. Sequence data from the Influenza Research Database (IRD; https://www.fludb.org) and GenBank (https://www.ncbi.nlm.nih.gov/genbank) were used for comparison. Black diamond indicates isolate from this study. Red text indicates candidate vaccine viruses. Blue text indicates H9N2/H7N9 sequences; green text indicates H6 subtypes; pink text indicates H5N1 subtypes; brown text indicates H5N6 subtypes. Scale bar indicates nucleotide substitutions per site.

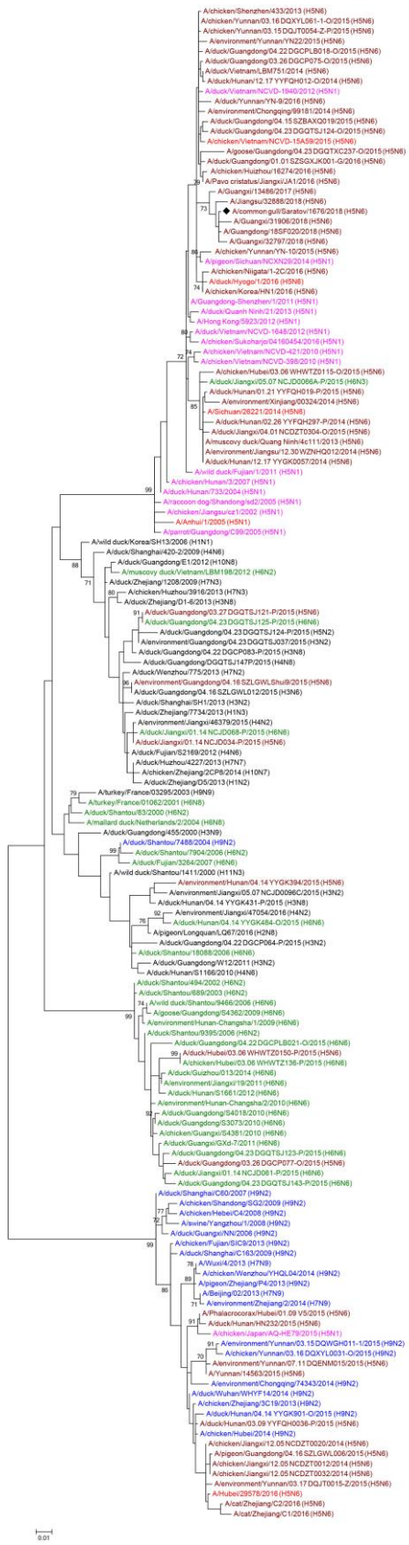


**Appendix Figure 7.** Phylogenetic analysis of the matrix (M) gene segment of A/common gull/Saratov/1676/2018 (H5N6) isolated from a common gull (*Larus canus*) in the Saratov Region of Russia, 2018. Phylogenetic analysis was performed by using MEGA version 6.0 (http://www.megasoftware.net) and the maximum likelihood method with 500 bootstrap replications. Numbers near the branches indicate bootstrap value >70%. Influenza virus sequences were deposited in Global Initiative on Sharing All Influenza Data (GISAID; https://platform.gisaid.org/epi3) under identification no. EPI1355418. Sequence data from the Influenza Research Database (IRD; https://www.fludb.org) and GenBank (https://www.ncbi.nlm.nih.gov/genbank) were used for comparison. Black diamond indicates isolate from this study. Red text indicates candidate vaccine viruses. Blue text indicates H9N2/H7N9 sequences; green text indicates H6 subtypes; pink text indicates H5N1 subtypes; brown text indicates H5N6 subtypes. Scale bar indicates nucleotide substitutions per site.

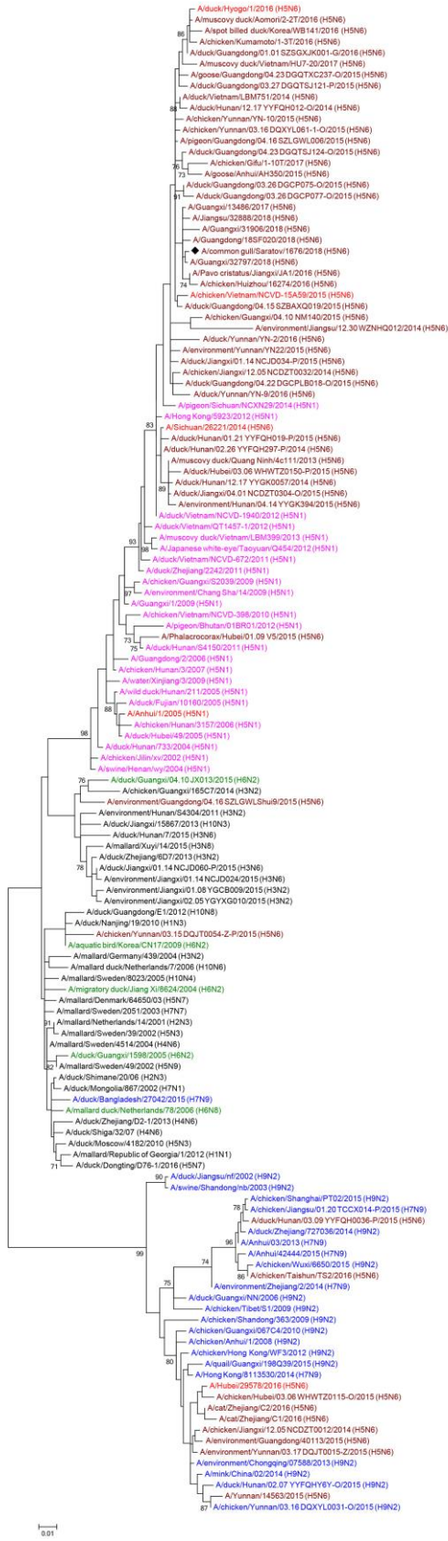


**Appendix Figure 8.** Phylogenetic analysis of the nonstructural protein (NSP) gene segment of A/common gull/Saratov/1676/2018 (H5N6) isolated from a common gull (*Larus canus*) in the Saratov Region of Russia, 2018. Phylogenetic analysis was performed by using MEGA version 6.0 (http://www.megasoftware.net) and the maximum likelihood method with 500 bootstrap replications. Numbers near the branches indicate bootstrap value >70%. Influenza virus sequences were deposited in Global Initiative on Sharing All Influenza Data (GISAID; https://platform.gisaid.org/epi3) under identification no. EPI1355418. Sequence data from the Influenza Research Database (IRD; https://www.fludb.org) and GenBank (https://www.ncbi.nlm.nih.gov/genbank) were used for comparison. Black diamond indicates isolate from this study. Red text indicates candidate vaccine viruses. Blue text indicates H9N2/H7N9 sequences; green text indicates H6 subtypes; pink text indicates H5N1 subtypes; brown text indicates H5N6 subtypes. Scale bar indicates nucleotide substitutions per site.

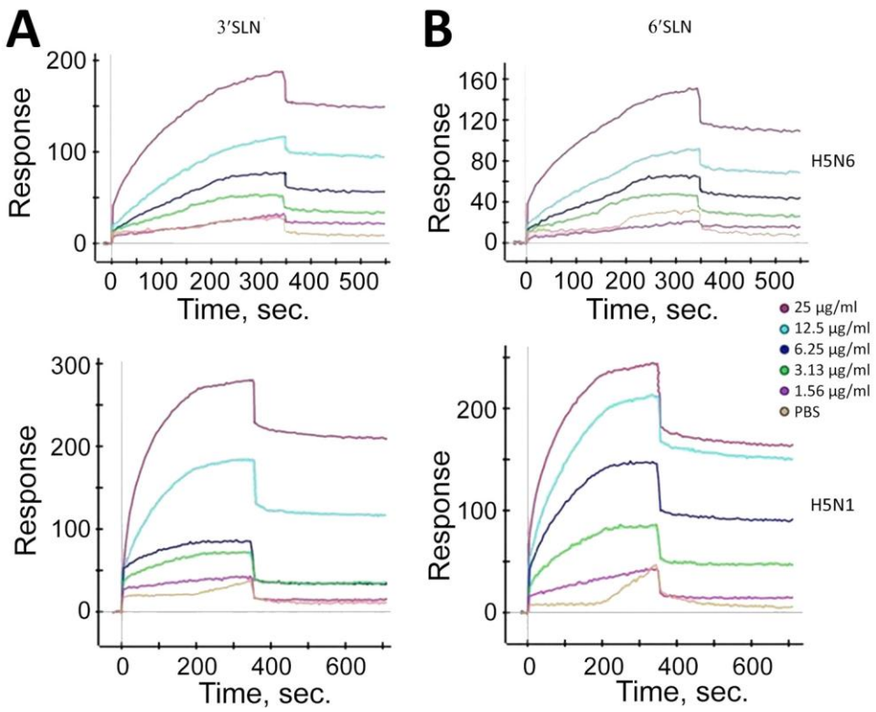


**Appendix Figure 9**. Surface plasma resonance sensorgrams for interaction of A/common gull/Saratov/1676/2018 (H5N6) and A/rook/Chany/32/2015 (H5N1) using receptor analogs for A) 3′SLN and B) 6′SLN after injection of viruses at the indicated concentrations. We used phosphate-buffered saline as a reference, which indicated specific binding between the virus and glycans. PBS, phosphate-buffered saline.